

Cite this: *Chem. Sci.*, 2025, 16, 16590

All publication charges for this article have been paid for by the Royal Society of Chemistry

Trends in organic peroxide (ROOR) formation in the reactions of C1–C4 alkyl peroxy radicals (RO₂) in gas

Barbara Nozière 

Organic peroxy radicals (RO₂) are important intermediates in aerobic systems such as Earth's atmosphere. The existence of a channel producing dialkyl peroxides (ROOR) in their self- and cross-reactions (*i.e.*, between the same or different radicals) has long been debated and considered a theoretical "key problem in the atmospheric chemistry of peroxy radicals". Over the past decade, observations have suggested that this channel could be an important source of condensable compounds and, ultimately, new aerosol particles in Earth's atmosphere. However, experimental evidence for specific RO₂ reactions is scarce. In this work, the formation of ROOR in the self- and cross-reactions of eight RO₂ (CH₃O₂, ¹³CH₃O₂, CD₃O₂, C₂H₅O₂, 1- and iso-C₃H₇O₂, 1- and *tert*-C₄H₉O₂) could be observed by modifying the ionisation conditions on a proton transfer mass spectrometer. The ROOR formation channel was confirmed to be in competition with the other product channels rather than precede them. For six of the RO₂ studied, the branching ratio, γ , for the ROOR channel of the self-reaction was quantified relative to these other channels. The results allowed for the first time to identify some trends in γ with respect to the RO₂ structure: γ decreases with increasing RO₂ chain length for the linear/primary radicals, ranging from (14.1 ± 7)% for CH₃O₂ to (1.1 ± 0.5)% for 1-C₄H₉O₂, while branched radicals exhibit much higher γ than their linear counterparts, with γ = (17.2 ± 8.6)% for iso-C₃H₇O₂ and (46.6 ± 23.2)% for *tert*-C₄H₉O₂. The formation of ROOR products from RO₂ reactions in the atmosphere should thus be strongly dependent on the RO₂ structure.

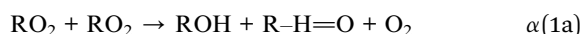
Received 16th May 2025
Accepted 8th August 2025

DOI: 10.1039/d5sc03559g

rsc.li/chemical-science

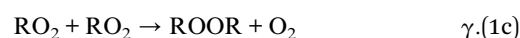
Introduction

Organic peroxy radicals (RO₂) are important intermediates in the oxidation of organic compounds in most aerobic chemical systems, such as biochemistry,^{1,2} chemical and food industry,^{3,4} low-temperature combustion,⁵ and Earth's atmosphere.^{6,7} Their main fates in most systems are reactions with other compounds or radicals, but their self-reactions and cross-reactions (*i.e.*, reactions between the same or different RO₂) can have non-negligible impacts in laboratory investigations. For most RO₂ radicals, the self-reaction is thought to involve at least two competing product channels:⁸



where ROH, R-H=O represent the alcohol and carbonyl products of RO₂, RO the corresponding alkoxy radical, and α and β the branching ratios of channels (1a) and (1b), respectively.

Some early works also reported the existence of a minor channel producing a peroxide: ROOR:⁹



However, the branching ratio for this channel, γ , was estimated to be small: $\gamma(\text{CH}_3\text{O}_2) \leq 6\%$, $\gamma(\text{C}_2\text{H}_5\text{O}_2) \leq 6\%$, $\gamma(\text{HOCH}_2\text{CH}_2\text{O}_2) \leq 2\%$, and $\gamma(\text{tert-C}_4\text{H}_9\text{O}_2) \leq 12\%$.⁹ For decades, no other study reported the observation of this channel and the latter was ruled out as negligible.^{6,9} Its existence was also difficult to explain theoretically and this channel was referred to as one of the "two key problems in the atmospheric chemistry of peroxy radicals".¹⁰ Over the past decade, laboratory investigations^{11,12} and atmospheric observations¹³ have reported the presence of "highly oxygenated molecules" (HOMs) in the gas phase, which systematically include "dimers" (*i.e.*, compounds having twice the number of C-atoms than their precursors). These compounds are expected to play important roles in the formation of new aerosol particles in the atmosphere. The dimers have been attributed to the self- and cross-reactions of RO₂,^{13,14} and these observations reignited the interest for this potential third channel of RO₂ + RO₂. Recent theoretical studies revealed new information on these reactions^{15–20} such as explaining the occurrence of the third

Royal Institute of Technology (KTH), Department of Chemistry, 114 28 Stockholm, Sweden. E-mail: noziere@kth.se



channel by intersystem crossing²⁰ and evidencing a fourth channel producing esters or ethers with complex RO₂.^{21,22} However, experimental data remain scarce. In recent years, the branching ratio γ has been quantified for the self-reactions of only four radicals (C₂H₅O₂,²³ CH₂(OH)CH₂O₂,²⁴ CH₃C(O)CH₂O₂,^{11,25} and C₃H₇O₂),²⁶ which does evidence any trend on how γ might vary with the RO₂ structure.

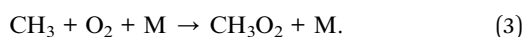
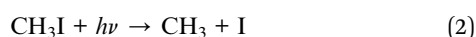
The present work investigates the formation of ROOR products in the self-reaction of eight RO₂ (CH₃O₂, ¹³CH₃O₂, CD₃O₂, C₂H₅O₂, 1- and iso-C₃H₇O₂, 1-C₄H₉O₂, *tert*-C₄H₉O₂) and in the cross-reactions of CH₃O₂ with C₂H₅O₂ and iso-C₃H₇O₂. In all experiments, radicals and products were monitored with a proton transfer chemical ionization mass spectrometer (CIMS), in which the ionization conditions were modified to enable ROOR detection. After checking the occurrence of the third channel in all of these reactions, the formation kinetics of ROOR were investigated, and the branching ratio γ was quantified.

Experimental section

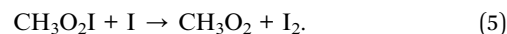
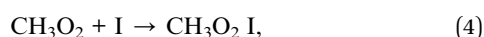
The experimental setup has been described in previous works.^{27,28} It consists of a vertical quartz reactor of total length $L = 120$ cm, in which organic peroxy radicals, RO₂, are produced photolytically by flowing a gas mixture through an irradiation window, corresponding to 2–8 s of residence time (see the “Radical production” section). After passing the irradiation window, the gas mixture flows in the dark, allowing further reactions to occur. In the present study, this part corresponded to reaction times between 0.5 and 10 s, which was achieved by moving the position of the irradiation window in the reactor. At the exit of the reactor, a small fraction (<10%) of the reaction mixture was sampled into a CIMS for analyses (see the “Detection” section). In this work, two nearly-identical reactors were used, with different internal diameters: $d = 3$ and 5 cm. The bath gas was synthetic air with a mass flow of 3.0 sLm, and the experiments were performed slightly below atmospheric pressure ($P = 0.85$ – 0.95 atm) and at room temperature ($T = 300 \pm 4$ K). The radical precursors were introduced into the main gas flow by bubbling a small flow of N₂ through the pure liquids and adding them to the reactor after a dilution loop. A list of the experiments performed in this work is given in Table S1 of the SI.

Radical production

The radicals were generated by the photolysis of iodinated precursors in a gas mixture flowing through an irradiation window. This irradiation window was surrounded by four narrow-band UV-C lamps (TUV 36W SLV/6; Phillips) emitting at $\lambda = 254$ nm. For instance, the RO₂, CH₃O₂, was produced by:



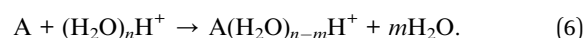
Note that the generation of I-atom led to side-reactions:²⁹



However, these fast reactions had negligible effects on most of the RO₂ studied in this work, except *tert*-C₄H₉O₂. The initial concentration of RO₂ in the different reactions was estimated to be between 1.5×10^{10} cm⁻³ (for 1-C₄H₉O₂) and 8×10^{13} cm⁻³ (for *tert*-C₄H₉O₂). Note that precise knowledge of the radical concentration was not necessary in this work.

Detection and quantification of radicals and products with the CIMS

This section only describes the general features of the detection of gas-phase compounds with the CIMS. The specific question of the ionization of ROOR is discussed in the “Results” section. Gas-phase compounds (“A” in reaction (6) below), including radicals and stable products, were ionized by proton transfer with the water clusters, (H₂O)_{*n*}H⁺, and detected with the CIMS:^{27,30–32}



Under the ionization conditions used in this study, the most abundant water/proton clusters were (H₂O)₃H⁺ (m/z 55) and (H₂O)₄H⁺ (m/z 73) rather than H₃O⁺. Thus, a compound of mass *M* was detected by its ion products at m/z *M* + 19, *M* + 37, and *M* + 55. The ion masses at which the radicals and products were monitored in this study are listed in Table S2.

In this work, the branching ratio γ for peroxide formation was quantified relative to the branching ratio α of channel (1a) or, in the case of *t*-C₄H₉O₂, to channel (1b) producing acetone. This quantification required the determination of the absolute concentration of all the compounds involved (*i.e.*, the alcohols, acetone, and ROOR), thus that of their detection sensitivity, S° (Hz ppb⁻¹). The detection sensitivities for methanol, ethanol, 1- and 2-propanol, 1-butanol, acetone, and di-*tert*-butyl peroxide were calibrated within $\pm 30\%$ using reference standards. The results are presented in Fig. S1 and showed that, within a class of compounds, S° decreases exponentially with the number of C-atoms and is smaller for the substituted compounds than for their linear counterparts. These trends are identical to those reported previously for a range of RO₂.³³ Therefore, for the ROOR, for which a standard was not available S° was estimated assuming the same trends than for the alcohols and RO₂. In practice, this meant that $S^\circ(\text{ROOR})$ was estimated by dividing S° for the corresponding alcohol by a factor of ~ 3 . This led to $\pm 50\%$ of uncertainties on the estimated S° values because of the wide range of values included in the extrapolation. These uncertainties propagated to the determination of the absolute concentrations for the ROOR in the experiments (except di-*tert*-butyl peroxide) and to the product ratios used to determine the branching ratio γ .

Chemicals

HiQ Synthetic air 5.0 was obtained from Linde Gas. NO (special mixture: 200 ppm in N₂), was purchased from Air Liquide. Iodomethane (CAS 74-88-4), 99.5%, was procured from

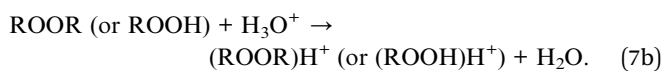
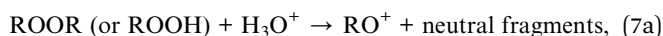


Chemtronica. Iodoethane (CAS 75-03-6), 99%, and 1-iodobutane (CAS 542-69-8), 98%, were obtained from ACROS/Fisher. The following chemicals were purchased from MilliporeSigma (formerly Sigma-Aldrich): iodomethane- D_3 (CAS 865-50-9), $\geq 99.5\%$; ^{13}C -iodomethane (CAS 4227-95-6), 99%; 1-iodopropane (CAS 107-08-4), $\geq 98.5\%$; 2-iodopropane (CAS 75-30-9), 99%; 2-iodo 2-methylpropane (CAS 558-17-8), 95%; di-*tert*-butyl peroxide (CAS 110-05-4), 98%; methanol (CAS 67-56-1), 99.8+%; ethanol (CAS 64-17-5), 99+%; 1-propanol (CAS 71-23-8), $\geq 99.9\%$; iso-propanol (CAS 67-63-0), 99.9%; 1-butanol (CAS 71-36-3), $\geq 99.0\%$; acetone (CAS 67-64-1), 99.0%.

Results and discussion

Favoring proton transfer over fragmentation in the detection of organic peroxides

Studies have reported that the ionisation of organic peroxides (ROOR) and hydroperoxides (ROOH) by proton transfer mass spectrometry proceeds exclusively by fragmentation (channel (7a) below) rather than by proton transfer (channel (7b)):³⁴



The ion fragment RO^+ is an isomer of the analog carbonyl ion (e.g., CH_3O^+ and $(\text{HCHO})\text{H}^+$ in the CH_3O_2 system; $\text{C}_2\text{H}_5\text{O}^+$ and $(\text{CH}_3\text{CHO})\text{H}^+$ in the $\text{C}_2\text{H}_5\text{O}_2$ system). Since carbonyl compounds are usually much more abundant than ROOR, the fragmentation precluded the detection of organic peroxides and hydroperoxides.

In this work, observing a standard of di-*tert*-butyl peroxide ($t\text{-C}_4\text{H}_9\text{Oot-C}_4\text{H}_9$) with the ionisation conditions used in our previous works to detect RO_2 (ref. 28 and 31) (i.e., a drift tube pressure of $P_{\text{drift}} = 10$ torr and electrical energy of $E/N \sim 45$ Td) led to distinct ion signals at m/z 165 and 183. These corresponded to the ions expected from proton transfer (Table S2) and indicated that this compound was, in fact, undergoing proton transfer in the CIMS. It was not possible to determine if the main ion for this compound was also undergoing fragmentation because the expected fragment RO^+ , m/z 73, overlapped with the most intense proton water cluster, $(\text{H}_2\text{O})_4\text{H}^+$. Thus, investigation of the proton transfer and fragmentation channels for ROOR was pursued with H_3COOCH_3 in the self-reaction of CH_3O_2 . The masses for the proton transfer and fragmentation ions for H_3COOCH_3 were m/z 81 and 99 (Table S2), and m/z 31, respectively, which allowed us to monitor both channels separately. Note that, under identical ionization conditions, HCHO was exclusively detected at m/z 67 and 85 (Table S2) and had a negligible signal at m/z 31, and therefore did not interfere with the monitoring of the fragment CH_3O^+ . The proton transfer and fragmentation channels of H_3COOCH_3 were then studied by maintaining the experimental conditions unchanged while varying the ionization conditions, mostly the electrical energy E/N (in Td) and drift tube pressure (Fig. 1). The fragmentation channel increased with the energy E/N and

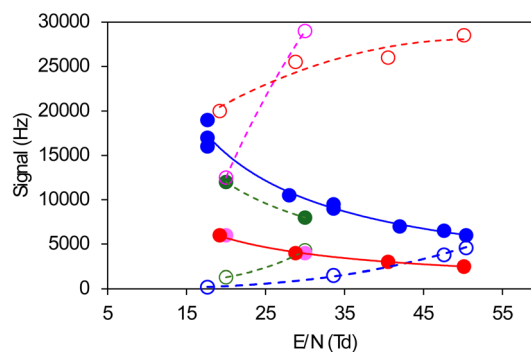


Fig. 1 Fragmentation and proton transfer channels for H_3COOCH_3 in a CIMS as a function of the ionization conditions (energy, E/N (in Td), and drift tube pressure). Open symbols = fragmentation channel monitored at m/z 31. Solid symbols = proton transfer channel, sum of m/z 81 and 99. Colors correspond to different pressures in the drift tube: blue = 20 torr; green = 15 torr; pink = 10 torr; red = 5 torr.

decreased with the drift tube pressure. Fragmentation dominated over proton transfer at and below 10 torr. This corresponds to the conditions in most commercial proton transfer mass spectrometers and to the fragmentation of organic peroxides reported in previous studies.³⁴ By contrast, proton transfer dominated over fragmentation at and above 15 torr. A drift tube pressure between 15 and 20 torr and an energy E/N between 15 and 35 Td were thus systematically used in this study to ensure that all the peroxides were detected by their proton transfer ions (Table S2).

Peroxide formation in the self- and cross-reactions of C1-C4 RO_2

In this work the self-reaction of eight RO_2 (CH_3O_2 , $^{13}\text{CH}_3\text{O}_2$, CD_3O_2 , $\text{C}_2\text{H}_5\text{O}_2$, 1- and iso- $\text{C}_3\text{H}_7\text{O}_2$, 1- $\text{C}_4\text{H}_9\text{O}_2$, *tert*- $\text{C}_4\text{H}_9\text{O}_2$) was studied as well as the cross-reactions of CH_3O_2 with $\text{C}_2\text{H}_5\text{O}_2$ and iso- $\text{C}_3\text{H}_7\text{O}_2$, producing ten different ROOR and ROOR'. The time profiles of these peroxides, along with those of the RO_2 , are presented in Fig. 2. To confirm the identity of the ROOR and exclude the contribution of pollution or other artefacts on the signals, each experiment included several cycles in which the lights were turned OFF (grey areas in Fig. 2) and at least one cycle with NO being added into the reactor (orange areas in Fig. 2). Studies of the cross-reactions with CH_3O_2 also involved several cycles in which the precursor (CH_3I) was turned ON/OFF. As shown in Fig. 2, the ROOR and RO_2 signals disappeared when the lights were off or when NO was added, confirming that the ROOR were products of RO_2 reactions. These cycles also indicated the background signal level to be subtracted when quantifying these compounds.

Observation of these ten different ROOR and ROOR' confirmed the universality of the peroxide-producing channel in these reactions.

Testing different formation mechanisms for ROOR

Next, the formation kinetics for ROOR were investigated to determine if this product resulted from the generally assumed



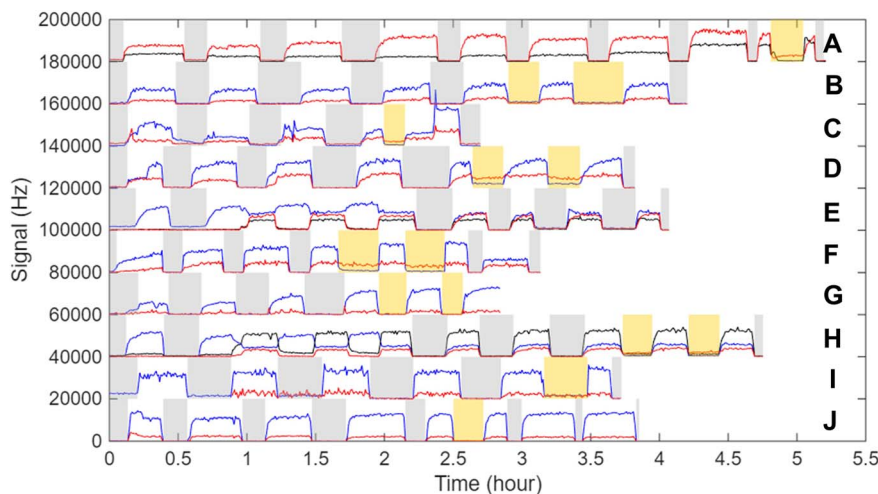
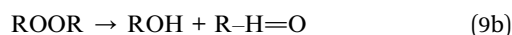
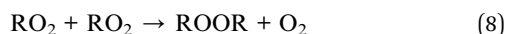


Fig. 2 Experimental signals for RO₂ and ROOR products. Grey areas: lights OFF. Orange areas: NO on. Black lines = CH₃O₂. Blue lines = other RO₂. Red lines = ROOR (and ROOR'). Signals have been scaled for clarity. (A) CH₃O₂ and H₃COOCH₃ (both × $\frac{1}{2}$). (B) CD₃O₂ and D₃COOCD₃ (both ×2). (C) ¹³CH₃O₂ and ¹³CH₃OO¹³CH₃ (×3). (D) C₂H₅O₂ and C₂H₅OOC₂H₅ (both ×2). (E) C₂H₅O₂, CH₃O₂ and C₂H₅OOCH₃. (F) 1-C₃H₇O₂ and 1-C₃H₇OOC₃H₇ (×3). (G) *i*-C₃H₇O₂ and *i*-C₃H₇OOC₃H₇ (×20). (H) *i*-C₃H₇O₂, CH₃O₂, and *i*-C₃H₇OOCH₃. (I) 1-C₄H₉O₂ (×2) and 1-C₄H₉OOC₄H₉ (×19). (J) *t*-C₄H₉O₂ (×1/2) and *t*-C₄H₉OOC₄H₉.

mechanism of reaction (1) (three parallel product channels, “Mechanism I”), or potentially from an alternative mechanism.

An alternative mechanism (“Mechanism II”) could be, for instance, the production of ROOR as the sole product in a first step (reaction (8) below), followed by its decomposition into the two other product channels (reaction (9)):



To determine which mechanism was taking place, kinetic simulations were performed using CH₃O₂ and *t*-C₄H₉O₂ as model RO₂, and compared with the experimental data (see details in Section S1). These simulations showed that, in all cases, Mechanism I resulted in a product ratio $R = [\text{ROH}]/[\text{ROOR}]$ and $R = [\text{acetone}]/[\text{ROOR}]$ not varying significantly over 0–10 s of reaction time (Fig. S2B and S3B–C). By contrast, Mechanism II led to the ratios R increasing by orders of magnitude over the same timescale (Fig. S2 and S3).

Experimental values for $R = [\text{ROH}]/[\text{ROOR}]$ and $R = [\text{acetone}]/[\text{ROOR}]$ in each experiment were obtained from the absolute concentrations of the alcohols, acetone, and peroxides. The latter were determined from the respective experimental signals, after subtraction of the background signal obtained in the absence of light. These net signals were then divided by the detection sensitivity, S° (Hz ppb⁻¹), determined as described in the Experimental section (*i.e.*, by direct calibration for the alcohols, acetone and di-*tert*-butyl peroxide, and by extrapolation from the known S° for the other ROOR). These product ratios, R , were then determined at different reaction times by moving the position of the irradiation window in the reactor. The results are presented in Fig. S5 and compared with the

kinetic simulations in Fig. S2B, C, S3C and D. Within the uncertainties (estimated to $\pm 50\%$), these experimental ratios did not vary significantly over 0–10 s of reaction time and, in any case, much less than expected from Mechanism II. These results clearly established that the mechanism governing the self-reaction of RO₂ was Mechanism I, as generally expected, in which the peroxide ROOR is formed in parallel with the other product channels.

Quantification of the peroxide yield, γ , in the self-reaction of RO₂

Once it was established that ROOR was produced in parallel to channel (1a) and (1b), the branching ratio γ was quantified from the product ratios R and the values of α or β recommended in the literature (see details in Section S2). To validate this approach, it was important to establish first that the product ratios did not vary significantly with the initial concentration of RO₂ (*i.e.*, between experiments for the same RO₂) and were mostly controlled by the relative branching ratios. This was verified by performing kinetic simulations with CH₃O₂ and *t*-C₄H₉O₂, in which [RO₂]₀ was varied by two orders of magnitude (Section S1 and Fig. S2B, S3B and C). In all cases, the product ratio, R , varied only by 20–25%. Thus, this ratio was not expected to vary within a series of experiments, where [RO₂]₀ varied by less than one order of magnitude. Relationships determining γ from the experimental product ratio, R , and the branching ratios α or β recommended in the literature were then established (see Section S2 for details). The expressions obtained were, for most RO₂:

$$\gamma = \alpha \times \frac{[\text{ROOR}]}{[\text{ROH}]} = \frac{\alpha}{R}, \quad (10)$$

and for *tert*-C₄H₉O₂



$$\gamma \approx 3\beta \times \frac{[\text{ROOR}]}{[\text{acetone}]} = \frac{\left(\frac{3}{R}\right)}{1 + \frac{3}{R}} \quad (11)$$

Using the experimental values for the ratio, R , determined above, γ was determined for the self-reaction of six of the eight RO_2 studied (Table 1 and Fig. 3). Note that γ was not quantified for CD_3O_2 and $^{13}\text{CH}_3\text{O}_2$ nor for the cross-reactions, mostly because the branching ratios for the other product channels in these reactions are not known, thus precluding the determination of γ , even if $[\text{ROH}]$ and $[\text{ROOR}]$ could be measured. In particular, the cross-reactions had four product channels ($\text{R}_1\text{O} + \text{R}_2\text{O}$, $\text{R}_1\text{OH} + \text{R}'_2 = \text{O}$, $\text{R}'_1 = \text{O} + \text{R}_2\text{OH}$, R_1OOR_2), for which none of the branching ratios is known.

The uncertainties in the branching ratios γ obtained were mostly those on the product ratios R . The latter were, in turn, a combination of the uncertainties on the alcohol (or acetone) and ROOR concentration.

The uncertainties on the absolute concentrations were mostly those on the detection sensitivity, S^0 , because the experimental signals were generally measured to $\pm 15\%$. However, the uncertainties on the ratio R were not the direct sum of those on the alcohol (or acetone) and ROOR concentrations because these partly compensated each other, especially because the detection sensitivity for most ROOR was estimated from that of the alcohols. Hence, the overall uncertainties on R (and, therefore, on γ) were assumed to result mostly from those on the detection sensitivities for the ROOR

Table 1 Determination of the branching ratio γ from the experimental ratio R and literature values for α

Expt. no.	RO_2	α	R_{obs}	γ	Average γ
PER1	CH_3O_2	0.48 ^a	3.3	0.147	
PER2	CH_3O_2	0.46 ^a	2.8	0.166	
PER3	CH_3O_2	0.46 ^a	2.7	0.170	
PER4	CH_3O_2	0.47 ^a	3.0	0.158	
PER5	CH_3O_2	0.55 ^a	6.7	0.082	
PER6	CH_3O_2	0.50 ^a	3.9	0.129	
PER7	CH_3O_2	0.49 ^a	3.5	0.140	0.141
PER8	$\text{C}_2\text{H}_5\text{O}_2$	0.3	3.3	0.091	
PER9	$\text{C}_2\text{H}_5\text{O}_2$	0.3	3.3	0.091	
PER10	$\text{C}_2\text{H}_5\text{O}_2$	0.3	4.4	0.071	
PER11	$\text{C}_2\text{H}_5\text{O}_2$	0.3	4.8	0.068	0.080
PER12	iso- $\text{C}_3\text{H}_7\text{O}_2$	0.44	2.8	0.259	
PER13	iso- $\text{C}_3\text{H}_7\text{O}_2$	0.44	15.3	0.050	
PER14	iso- $\text{C}_3\text{H}_7\text{O}_2$	0.44	3.9	0.207	0.172
PER15	1- $\text{C}_3\text{H}_7\text{O}_2$	0.3 ^b	5.1	0.055	
PER16	1- $\text{C}_3\text{H}_7\text{O}_2$	0.3 ^b	11.6	0.031	
PER17	1- $\text{C}_3\text{H}_7\text{O}_2$	0.3 ^b	12.6	0.029	0.038
PER18	1- $\text{C}_4\text{H}_9\text{O}_2$	0.3 ^b	27.4	0.011	
PER19	1- $\text{C}_4\text{H}_9\text{O}_2$	0.3 ^b	31.0	0.010	
PER20	1- $\text{C}_4\text{H}_9\text{O}_2$	0.3 ^b	25.2	0.012	0.011
PER21	<i>tert</i> - $\text{C}_4\text{H}_9\text{O}_2$	—	3.24	0.481	
PER22	<i>tert</i> - $\text{C}_4\text{H}_9\text{O}_2$	—	3.06	0.495	
PER23	<i>tert</i> - $\text{C}_4\text{H}_9\text{O}_2$	—	3.51	0.461	
PER24	<i>tert</i> - $\text{C}_4\text{H}_9\text{O}_2$	—	4.00	0.429	0.466

^a Calculated from β from ref. 9 and R . ^b Assumed identical to α for $\text{C}_2\text{H}_5\text{O}_2$.

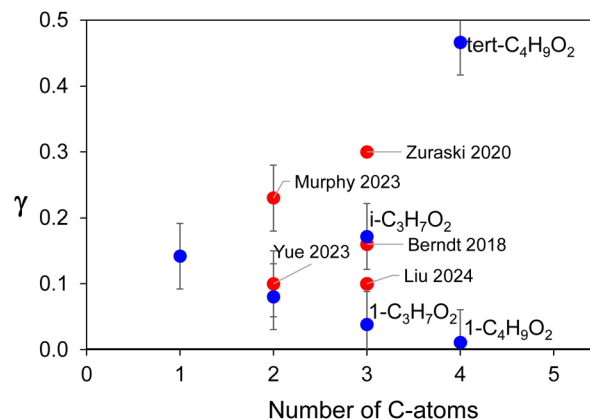


Fig. 3 Branching ratio, γ , for the formation of ROOR in the self-reactions of RO_2 studied in this work (blue symbols) and comparison with literature data (red symbols).

i.e., $\pm 50\%$. The lack of variation of the ratio, R , with reaction time and the initial radical concentration makes this methodology for quantifying γ robust. Relying on concentration ratios also compensated, to a certain extent, for the variability in the ionisation conditions between experiments.

All the branching ratios measured in this work are larger than those recommended in the IUPAC database:⁹ 14.1% (instead of $\leq 6\%$) for CH_3O_2 , 8.0% (instead of $\leq 6\%$) for $\text{C}_2\text{H}_5\text{O}_2$, and 46.6% (instead of $\leq 2\%$) for *tert*- $\text{C}_4\text{H}_9\text{O}_2$. These differences could be attributed to the difficulty in observing and quantifying ROOR compounds with multiple analytical methods.

The branching ratios reported here for six RO_2 allow, for the first time, to distinguish some trends in the variation of γ with the RO_2 structure. Two trends are visible in Fig. 3: (i) a decrease in γ with increase in the number of C-atoms for the linear/primary alkyl RO_2 ; (ii) larger γ for the branched RO_2 than for the linear counterparts. Thus, peroxide formation seems to be a minor channel for linear/primary RO_2 (except perhaps CH_3O_2) and mostly significant for substituted ones.

The value of $\gamma = 8 \pm 4\%$ obtained in this work for the peroxide of $\text{C}_2\text{H}_5\text{O}_2$ agrees well with the previous determination of $\gamma = 10 \pm 5\%$ ²³ for this compound (Fig. 3). The values of $\gamma = 3.8 \pm 1.9\%$ obtained for the peroxide of 1- $\text{C}_3\text{H}_7\text{O}_2$ and $\gamma = 17.2 \pm 8.6\%$ for *i*- $\text{C}_3\text{H}_7\text{O}_2$ are consistent with $\gamma = 10 \pm 5\%$ reported previously for a mixture of both compounds.²⁶ Larger branching ratios have also been reported for functionalized RO_2 compared with the corresponding alkyl RO_2 : $\gamma = 23 \pm 5\%$ for the peroxide of $\text{HOCH}_2\text{CH}_2\text{O}_2$ (ref. 24), thus larger than for $\text{C}_2\text{H}_5\text{O}_2$, and $\gamma = 16 \times 2/2\%$ (ref. 11) and $30 \times 2/2\%$ (ref. 25) for that of $\text{CH}_3\text{C}(\text{O})\text{CH}_2\text{O}_2$, both larger than for 1- $\text{C}_3\text{H}_7\text{O}_2$. This comparison shows that, beside substitution, some functionalization also enhances the formation yield of ROOR.

Conclusions and atmospheric implications

By exploring the self- and cross-reactions of eight RO_2 , we confirmed the general existence of a channel producing ROOR



in these reactions. Our experimental data indicate that peroxides are formed in parallel to the other product channels, and do not precede them. The branching ratios, γ , measured for six of the RO₂ studied were all larger than those recommended in databases.⁹ These results reveal some distinct trends in γ with radical structure: a decrease with increasing radical size for linear and primary RO₂, and larger γ for branched radicals relative to their linear counterparts. Thus, the formation of ROOR is expected to be small for most linear/primary RO₂, and mostly significant for branched ones. A comparison of these results with literature data for peroxide formation from functionalized RO₂ also show that functionalization enhances this channel compared with the linear alkyl analogs.

Because of the relative abundance of CH₃O₂ in the atmosphere, the branching ratio $\gamma = 14.1 \pm 7\%$ reported in this work might result in non-negligible concentration of its peroxide in low-NO_x regions. Cross-peroxides between CH₃O₂ and other RO₂ would also be favored in such environments. Otherwise, the formation of organic peroxides from RO₂ self- and cross-reactions in the atmosphere is expected to be mostly important for large ($C \geq 5$) and substituted RO₂ resulting from organic precursors of global importance, such as isoprene and terpenes.²⁴ The competition between RO₂ self- and cross-reactions and their other reactions (with NO, HO₂...) in the atmosphere is likely to be the main limit for the formation of organic peroxides by these pathways. Other potential formation mechanisms could be considered for these compounds, such as condensed-phase or surface reactions.³⁵

Author contributions

Funding acquisition, methodology, experimental, writing: BN.

Conflicts of interest

There are no conflicts of interest to declare.

Data availability

The raw data of our experiments is posted on Zenodo at <https://doi.org/10.5281/zenodo.16672804> and is freely available.

Some of the data supporting the work presented are provided in the SI. See DOI: <https://doi.org/10.1039/d5sc03559g>.

Acknowledgements

Professor Zoltan Zsabo, KTH, is warmly acknowledged for performing NMR of ¹³CH₃I and CD₃I standards. M. Sylvain Miquet, Université Paris-Saclay, France, is gratefully acknowledged for generating Fig. 2 in Matlab. This work was part of the ERC Advanced Grant Project EPHEMERAL (884532) and has received funding from the European Research Council under the Horizon 2020 Research And Innovation Programme of the European Union.

Notes and references

- 1 B. Halliwell and J. M. Gutteridge, *Free radicals in biology and medicine*, Oxford university press, USA, 2015.
- 2 M. Valko, K. Jomova, C. J. Rhodes, K. Kuča and K. Musilek, *Arch. Toxicol.*, 2016, **90**, 1.
- 3 E. Choe and D. B. Min, *Compr. Rev. Food Sci. Food Saf.*, 2009, **8**, 345.
- 4 M. Brewer, *Compr. Rev. Food Sci. Food Saf.*, 2011, **10**, 221.
- 5 F. Battin-Leclerc, *Prog. Energy Combust. Sci.*, 2008, **34**, 440.
- 6 J. J. Orlando and G. S. Tyndall, *Chem. Soc. Rev.*, 2012, **41**, 6294.
- 7 M. J. Goldman, W. H. Green and J. H. Kroll, *J. Phys. Chem. A*, 2021, **125**, 10303.
- 8 P. D. Lightfoot, R. A. Cox, J. N. Crowley, M. Destriau, G. D. Hayman, M. E. Jenkin, G. K. Moortgat and F. Zabel, *Atmos. Environ., Part A*, 1992, **26**, 1805.
- 9 R. Atkinson, D. L. Baulch, R. A. Cox, J. N. Crowley, R. F. Hampson, R. G. Hynes, M. E. Jenkin, M. J. Rossi and J. Troe, *Atmos. Chem. Phys.*, 2006, **6**, 3625.
- 10 T. S. Dibble, *Atmos. Environ.*, 2008, **42**, 5837.
- 11 T. Berndt, W. Scholz, B. Mentler, L. Fischer, H. Herrmann, M. Kulmala and A. Hansel, *Angew. Chem., Int. Ed.*, 2018, **57**, 3820.
- 12 T. Berndt, B. Mentler, W. Scholz, L. Fischer, H. Herrmann, M. Kulmala and A. Hansel, *Environ. Sci. Technol.*, 2018, **52**, 11069.
- 13 T. Jokinen, M. Sipilä, S. Richters, V.-M. Kerminen, P. Paasonen, F. Stratmann, D. Worsnop, M. Kulmala, M. Ehn, H. Herrmann and T. Berndt, *Angew. Chem., Int. Ed.*, 2014, **53**, 14596.
- 14 M. Ehn, J. A. Thornton, E. Kleist, M. Sipilä, H. Junninen, I. Pullinen, M. Springer, F. Rubach, R. Tillmann and B. Lee, *Nature*, 2014, **506**, 476.
- 15 R. R. Valiev, G. Hasan, V.-T. Salo, J. Kubecka and T. Kurtén, *J. Phys. Chem. A*, 2019, **123**, 6596.
- 16 G. Hasan, V.-T. Salo, R. R. Valiev, J. Kubecka and T. Kurtén, *J. Phys. Chem. A*, 2020, **124**, 8305.
- 17 V.-T. Salo, R. Valiev, S. Lehtola and T. Kurtén, *J. Phys. Chem. A*, 2022, **126**, 4046.
- 18 C. D. Daub, R. Valiev, V.-T. Salo, I. Zakai, R. B. Gerber and T. Kurtén, *ACS Earth Space Chem.*, 2022, **6**, 2446.
- 19 V.-T. Salo, J. Chen, N. Runeberg, H. G. Kjaergaard and T. Kurtén, *J. Phys. Chem. A*, 2024, **128**, 1825.
- 20 I. Mandal, C. D. Daub, R. Valiev, T. Kurtén and R. B. Gerber, *Phys. Chem. Chem. Phys.*, 2025, **27**, 2395.
- 21 O. Perakyla, T. Berndt, L. Franzone, G. Hasan, M. Meder, R. R. Valiev, C. D. Daub, J. G. Varelas, F. M. Geiger and R. J. Thomson, *J. Am. Chem. Soc.*, 2023, **145**, 7780.
- 22 L. Franzone, M. Camredon, R. Valorso, B. Aumont and T. Kurtén, *Atmos. Chem. Phys.*, 2024, **24**, 11679.
- 23 H. Yue, C. Zhang, X. Lin, Z. Wen, W. Zhang, S. Mostafa, P.-L. Luo, Z. Zhang, P. Hemberger and C. Fittschen, *Int. J. Mol. Sci.*, 2023, **24**, 3731.
- 24 S. E. Murphy, J. D. Crouse, K. H. Møller, S. P. Rezgui, N. J. Hafeman, J. Park, H. G. Kjaergaard, B. M. Stoltz and P. O. Wennberg, *Environ. Sci.: Atmos.*, 2023, **3**, 882.



- 25 K. Zuraski, A. O. Hui, F. J. Grieman, E. Darby, K. H. Møller, F. A. Winiberg, C. J. Percival, M. D. Smarte, M. Okumura and H. G. Kjaergaard, *J. Phys. Chem. A*, 2020, **124**, 8128.
- 26 L. Liu, C. Zhang, Y. Xia, W. Zhang, Z. Wang and X. Tang, *Chemosphere*, 2024, **363**, 142846.
- 27 B. Nozière and F. Fache, *Chem. Sci.*, 2021, **12**, 11676.
- 28 B. Nozière and L. Vereecken, *Phys. Chem. Chem. Phys.*, 2024, **26**, 25373.
- 29 T. J. Dillon, M. E. Tucceri and J. N. Crowley, *Phys. Chem. Chem. Phys.*, 2006, **8**, 5185.
- 30 D. Hanson, J. Orlando, B. Noziere and E. Kosciuch, *Int. J. Mass Spectrom.*, 2004, **239**, 147.
- 31 B. Nozière and D. R. Hanson, *J. Phys. Chem. A*, 2017, **121**, 8453.
- 32 A. M. Ellis and C. A. Mayhew, *Proton transfer reaction mass spectrometry: principles and applications*, John Wiley & Sons, 2013.
- 33 B. Nozière and L. Vereecken, *Angew. Chem., Int. Ed.*, 2019, **58**, 13976.
- 34 H. Li, T. G. Almeida, Y. Luo, J. Zhao, B. B. Palm, C. D. Daub, W. Huang, C. Mohr, J. E. Krechmer and T. Kurtén, *Atmos. Meas. Tech. Discuss.*, 2021, **2021**, 1.
- 35 V. Vasudevan-Geetha, L. Tiszenkel, Z. Wang, R. Russo, D. Bryant, J. Lee-Taylor, K. Barsanti and S. H. Lee, *EGUsphere*, 2024, vol. 2024, p. 1, DOI: [10.5194/egusphere-2024-2454](https://doi.org/10.5194/egusphere-2024-2454).

